Quaternary Structure of the HSC70 Cochaperone HIP†

Marion Velten,‡ Bruno O. Villoutreix,§ and Moncef M. Ladjimi*,‡

Laboratoire de Biochimie des Signaux Régulateurs Cellulaires et Moléculaires, UMR 7631, CNRS-Université Pierre et Marie Curie, 96 Boulevard Raspail, Paris, France, and The Wallenberg Laboratory, Department of Clinical Chemistry, Lund University, University Hospital, S-205 02 Malmö, Sweden

Received July 28, 1999; Revised Manuscript Received October 20, 1999

ABSTRACT: HSC70 interacting protein (HIP) is an essential cytoplasmic cochaperone involved in the regulation of HSC70 chaperone activity and the maturation of progesterone receptor. To determine the quaternary structure and the gross conformation of the protein in solution, a wide array of biochemical and biophysical techniques has been used. Size-exclusion chromatography and sedimentation velocity indicate the presence of a single species with a Stokes radius, R_s, of 55 Å and a sedimentation coefficient, $s^\circ_{20,w}$, of 4.34 S. The combination of these data gives a molecular mass of 101 000 Da, a value close to that of the theoretical molecular mass of a dimer (87 090 Da). Sedimentation equilibrium, performed at various protein concentrations and rotor speeds, gives a molecular mass of 88 284 Da, almost in exact agreement with the molecular mass of a dimer. On the basis of these data, a frictional ratio f/f_0 of 1.6 is obtained, suggesting an elongated shape for the HIP dimer. Secondary structure predictions, supported by circular dichroism experiments, indicate that HIP is an almost all α-protein, able to form extended coiled coils. Using threading and comparative model building methods, a structural model of a segment of HIP involved in HSC70 binding has been constructed and potential sites of interaction between HIP and HSC70 are proposed on the basis of electrostatic as well as shape complementarity. Altogether, these results indicate that HIP is an elongated dimer, able to bind two HSC70 molecules through its TPR regions, and suggest the existence of a versatile binding site on HSC70 that may be involved in the interaction of the chaperone with the cochaperones or other interacting proteins.

Molecular chaperones of the 70 kDa heat shock protein (HSP70)[1] family play an essential role in protein folding, assembly, transport, degradation, and signal transduction (for reviews, see refs *1*−*4*). They are thought to act by transiently binding hydrophobic regions exposed to the solvent in the non-native or unassembled states of proteins, thereby preventing off-pathway reactions that lead to unproductive folding or aggregation (*5*−*8*).

HSP70s seem to function through cycles of binding and hydrolysis of ATP coupled to cycles of binding and release of polypeptide substrate (*9*). In the ATP form, HSP70 exhibits fast kinetics and low affinity, whereas in the ADP form, it exhibits slow kinetics and a high affinity for binding polypeptide substrates (*10*, *11*). Cycling between these two forms depends on the efficiency of ATP hydrolysis and that of ADP to ATP exchange, and is modulated by regulatory proteins called cochaperones (*9*). Several models, based on the *Escherichia coli* DnaK−DnaJ−GrpE system, have been proposed to account for HSP70's switching and substrate binding properties. Briefly, in these models, the cochaperone DnaJ activates the hydrolysis of ATP by DnaK, thereby stabilizing the protein in its high-affinity ADP form, while the cochaperone GrpE stimulates the exchange of ADP with ATP, thus helping the protein to switch back to its low-affinity ATP form (*9*−*11*).

While eukaryotic homologues of the DnaK-ATPase stimulation factor DnaJ have been found in all cell compartments (*12*), eukaryotic homologues of the ADP−ATP exchange factor GrpE appeared to be restricted to mitochondria and chloroplasts, two organelles of prokaryotic origin (*13*). Thus, the absence of a GrpE homologue in the cytosol of eukaryotes precluded the generalization of the DnaK−DnaJ−GrpE chaperone−cochaperone model system. It is in fact in a search for HSC70 interacting proteins in eukaryotic cytosol, using the two-hybrid system, that HIP (HSC70 interacting protein) has been isolated (*14*). This protein has also been identified, in an independent manner, in complexes with HSC70 and HSP90, as a factor that transiently associates with progesterone receptor (*15*).

HIP, a protein with 368 residues, regulates HSC70 chaperone activity by binding to its N-terminal domain and stabilizing the protein in its ADP form which has a high affinity for the polypeptide substrates (*14*). The protein is composed of an N-terminal domain (residues 1−100) that is responsible for the protein oligomerization, a central, tetratricopeptide repeat (TPR)-containing domain (residues 113−214) involved in HSC70 binding, and a GGMP-rich, C-terminal domain (residues 281−368) with unknown func-

† This work was supported in part by the Association pour la Recherche sur le Cancer (ARC), the Ligue Nationale Contre le Cancer, and the Fondation pour la Recherche médicale (FRM). M.V. is supported by an MENRT predoctoral fellowship.

* Corresponding author. Telephone: 33 1 53 63 40 90. Fax: 33 1 42 22 13 98. E-mail: ladjimi@ccr.jussieu.fr.

‡ CNRS-Université Pierre et Marie Curie.

§ Lund University.

[1] Abbreviations: HSC70, 70 kDa heat shock cognate protein; HSP70, 70 kDa heat shock protein; HIP, HSC70 interacting protein; TPR, tetratricopeptide repeat.

10.1021/bi9917535 CCC: $19.00
Published on Web 12/15/1999

tion (*16*, *17*).

HIP appears not to be homologous with GrpE either structurally or functionally and exhibits rather the opposite activity (*14*). Although intriguing, this finding has been rationalized by the fact that ADP release is not the rate-limiting step in the eukaryotic, constitutive HSP70 cycle, by contrast to the bacterial HSP70 cycle, and can occur in the absence of a GrpE homologue (*18*, *19*). Yet, other proteins that interact with HSC70, such as p60 (HSC70 organizing protein, HOP) and BAG-1, that were found to have nucleotide exchange activity have been proposed to functionally substitute for GrpE even though they are structurally distinct from it (*20*, *21*).

In an effort to gain a better understanding of the eukaryotic HSP70 chaperone−cochaperone system, we have undertaken the characterization of the structural properties of the different components of this system either separately or in complexes with other partners. We report here the structural analysis of HIP in dilute solution and a description of its hydrodynamic properties. A structural model of the TPR region of HIP and a potential binding site on HSC70 are proposed.

EXPERIMENTAL PROCEDURES

Materials

FPLC products and columns were from Amersham-Pharmacia Biotech, and nickel−agarose and IPTG were from Novagen. Protease inhibitors were purchased from Boehringer, and all other chemicals from Merck or Sigma.

Methods

HIP Expression and Purification. HIP was expressed from a pET vector (kindly provided by J. Höhfeld and F.-U. Hartl) encoding HIP fused to a Myc epitope followed by a histidine tag at the carboxy-terminal extremity (*14*). A pET vector expressing HIP fused to a histidine tag at the amino-terminal extremity was also constructed, and gave results similar to those of the vector provided by J. Höhfeld and F.-U. Hartl. BL21 *E. coli* cells bearing this plasmid were incubated overnight in 20 mL of LB medium containing 200 μg/mL ampicillin at 37 °C with vigorous shaking. After 100-fold dilution of the culture in the same medium and growth to an OD_{600} of 0.6, expression of the protein was induced by the addition of 0.5 mM isopropyl 1-thio-β-D-galactopyranoside (IPTG), and the cells were further incubated for 4 h at 37 °C. Cells were recovered after centrifugation at 5000*g* for 10 min at 4 °C, and resuspended in 15 mL of binding buffer [20 mM Tris-HCl (pH 7.9), 1 M NaCl, and 5 mM imidazole] supplemented with 1 mM PMSF, 2.5 μM bestatin, 50 μM orthophenanthroline, 11 μM amastatin, and 0.5 μg/mL leupeptin.

After sonication, the lysate was cleared by two successive centrifugations (30 min and 1 h) at 40000*g* at 4 °C and then loaded onto a 5 mL nickel−agarose column pre-equilibrated with 3 volumes of binding buffer at a flow rate of 0.2 mL/min. The column was then washed with 10 volumes of binding buffer, followed by 8 volumes of washing buffer (binding buffer with 45 mM imidazole). HIP was eluted using an imidazole gradient (45 to 200 mM), and fractions (2 mL) were collected. The fractions containing HIP were pooled, and the buffer was changed through successive cycles of concentration and dilution in an ultrafiltration cell (YM10 membrane, Amicon). Further purification was achieved using a 25 mL Source 30Q anion exchange column (Amersham-Pharmacia Biotech) equilibrated with buffer A [20 mM Tris-HCl (pH 8.3), 20 mM NaCl, 1 mM β-mercaptoethanol, and 1 mM EDTA] at a flow rate of 0.5 mL/min. The column was washed with 2 volumes of buffer A, and then eluted with a NaCl gradient (20 to 300 mM). Among the three different peaks containing HIP, only the central peak was recovered as it consists of homogeneous protein. HIP was then concentrated by ultrafiltration (YM10 membrane, Amicon), and stored in buffer B [20 mM Tris-HCl (pH 7.5), 100 mM NaCl, 1 mM β-mercaptoethanol, and 1 mM EDTA] at −80 °C. The protein concentration was determined by the method of Lowry using bovine serum albumin as a standard.

Electrophoresis. Polyacrylamide gel electrophoresis (PAGE) under denaturing conditions (SDS) was carried out in 0.75 mm thick 12% acrylamide slab gels according to the method of Laemmli (*22*). Gels were run using the Mini-Protean II apparatus from Bio-Rad. PAGE under native conditions was performed on 6% acrylamide slab gels according to the method of Kim et al. (*23*).

Size-Exclusion Chromatography. Size-exclusion chromatography experiments were carried out at room temperature using an AKTA-FPLC system (Amersham Pharmacia Biotech). Samples of HIP in buffer B were loaded on a Superdex 200 HR10/30 column (Amersham Pharmacia Biotech) pre-equilibrated in buffer B. Fractions (0.5 mL) were collected at a flow rate of 0.4 mL/min, and the absorbance was measured at 280 nm. Fractions were then lyophilized and analyzed by SDS−PAGE. The column was calibrated with a calibration kit from Amersham Pharmacia Biotech with Stokes radii ranging from 16.4 Å (13.7 kDa) to 85 Å (669 kDa).

Proteins with known molecular masses and Stokes radii were used for the calibration curve representing the Stokes radius as a function of the distribution coefficient K_{av} (*24*, *25*). The standards were ferritin (MW = 440 kDa, R_s = 61 Å), catalase (MW = 232 kDa, R_s = 52.2 Å), aldolase (MW = 158 kDa, R_s = 48.1 Å), albumin (MW = 67 kDa, R_s = 35.5 Å), ovalbumin (MW = 43 kDa, R_s = 30.5 Å), chymotrypsinogen A (MW = 25 kDa, R_s = 20.9 Å), and RNase A (MW = 13.7 kDa, R_s = 16.4 Å).

The HIP molecular mass could be estimated by a combination of the Svedberg and Stokes equations, using the Stokes radius and the sedimentation coefficient.

Rhodanese Aggregation Assay. Rhodanese was denatured in 6 M guanidinium hydrochloride and 30 mM Tris-HCl (pH 7.5) at 25 °C for 1 h and then diluted 100-fold to a final concentration of 0.5 μM in 20 mM Tris-HCl (pH 7.5) and 100 mM NaCl, in the presence or absence of HIP or BSA as a control. The turbidity of the samples under constant agitation was measured at 320 nm over the course of 20 min at 25 °C.

Circular Dichroism. The CD spectrum of HIP was measured at 25 °C using 4.6 μM protein, in 25 mM sodium phosphate (pH 7), on a Jobin-Yvon Mark V dichrograph and 2 mm wide cuvettes. All spectra were recorded with a 0.2 nm step and corrected for the baseline. These measurements are reported as mean residue ellipticity [θ] (degrees per square centimeter per decimole). The relative content in α-helix was estimated according to ref *26* from the $\Delta\epsilon$ at

222 nm and by deconvolution of the spectrum and comparison with proteins with known secondary structure content.

Sedimentation Velocity. Sedimentation velocity experiments were performed on a Beckman Optima XL-A analytical ultracentrifuge equipped with a AnTi 60 titanium four-hole rotor with two-channel 12 mm path-length centerpieces, as previously described (*27*). The compartments were filled with 400 μL of HIP at three different concentrations (0.3, 0.6, and 1.2 mg/mL) in buffer B and centrifuged at 55 000 rpm at 4 °C. Radial scans of the absorbance at 280 nm were taken at 6 min intervals, and experimental baselines were measured for each sample at the end of the run. HIP remained stable over the course of the run as shown by SDS−PAGE before and after the run. Data analysis was performed using g(s) (*28*) and SVEDBERG (*29*) computer programs.

Hydrodynamic parameters were evaluated using the program SEDNTERP (*30*). The molecular mass of the monomer (43 545 Da) and the partial specific volume, $\bar{v}$, 0.72 cm^3/g (at 4 °C), were calculated from the amino acid composition, while the solvent density, ρ, 1.00462 g/cm^3 (at 4 °C), was obtained from SEDNTERP. The amino acid composition takes into account the addition of the Myc epitope and the histidine tag at the C-terminus of the authentic protein. The degree of hydration of the protein, 0.504 g of H_2O/g of protein, was estimated, on the basis of the amino acid composition, by the method of Kuntz, (*31*) according to Laue et al. (*30*). However, since this value is calculated for a totally unfolded protein in which all the amino acids are exposed to solvent, and tends therefore to be overestimated, a correction factor is necessary to account for internal residues that are not accessible to solvent. A correction factor of 0.7 is obtained by comparing degrees of hydration for several proteins in their folded state to that based on their amino acid composition (*32*). Thus, a degree of hydration of 0.35 g of H_2O/g of protein was used for the calculation of the axial ratio a/b of the hydrodynamically equivalent prolate ellipsoid of revolution. The diffusion coefficient D was estimated using the Stokes radius, by means of the Einstein relation (*30*). The frictional ratio f/f_0 was calculated using the corrected sedimentation coefficient $s^\circ_{20,w}$ and the molecular mass obtained by sedimentation equilibrium analysis (*30*).

Sedimentation Equilibrium. The molecular mass of HIP was determined by sedimentation equilibrium analysis at 4 °C using three loading concentrations (0.3, 0.6, and 1.2 mg/mL in buffer B) and three rotor speeds (6000, 9000, and 14 000 rpm). Radial scans of the absorbance at 280 nm were taken at 3 h intervals, and samples were judged to be at equilibrium by the absence of systematic deviations in overlayed successive scans, and when a constant average molecular mass (MW) was obtained in plots of MW versus centrifugation time. HIP remained stable over the course of the run as shown by SDS−PAGE before and after the run.

Multiple data sets were analyzed by nonlinear least-squares procedures provided in the Beckman Optima XL-A software package (*33*). The baseline offset was obtained from menisc depletion of the sample at 40 000 rpm at the end of the run. Data analysis was performed using the following general equation:

$$C(r) = \delta + C(r_0)\exp[\sigma(r^2 - r_0^2)]$$

where $C(r)$ is the total concentration at radius r, δ the baseline offset, and $C(r_0)$ the monomer concentration at the reference radius r_0. σ is defined as

$$\sigma = M(1 - \bar{v}\rho)\omega^2/2RT$$

where M is the monomer molecular weight, $\bar{v}$ the partial specific volume, ρ the solvent density, ω the angular velocity of the rotor, R the gas constant, and T the absolute temperature of the sedimentation equilibrium experiment.

Protein Modeling. The InsightII/homology/biopolymer/Discover/DelPhi program package (Biosym-MSI) was used for the construction of the model.

(1) Selection of a Structural Template for HIP. The UCLA-DOE fold recognition server (*34*) was used to identify putative structural templates upon which to build a model for HIP. The TPR domain of the phosphatase 5 (PP5) X-ray structure (*35*) was selected as the initial template. Conservative side chain replacements were modeled in conformations similar to the ones present in the PP5 structure. Other residue replacements were modeled using the PP5 coordinates as the initial template and optimized, if needed, using low-energy rotamer conformations (*36*). Low-energy rotamers were calculated using an 8 Å cutoff distance for nonbonded interactions.

(2) Energy Refinement and Validation of the Model. The HIP model was then energy minimized using Discover (Biosym-MSI). All calculations were carried out using the CVFF parameters, a dielectric constant of 1, and a 20 Å cutoff distance for nonbonded interactions. Hydrogen atoms were added to the model, and partial charges were assigned to all atoms. The model was then refined in a stepwise fashion, starting with all heavy atoms tethered to their original positions and then relaxed. The stereochemistry of the model was analyzed using ProStat (Biosym-MSI). The final model bond lengths, backbone Ω angles, side chain χ_1 and χ_2 angles, and chirality showed no unusual structural features, indicative of the appropriateness of the modeling strategy and the overall accuracy of the model. Most ϕ and ψ angles on the Ramachandran plot were within the energetically favored regions. No steric clashes were observed despite the low degree of sequence identity between HIP and PP5, further supporting the hypothesis that these two proteins are structurally very similar in this region. Charged residues were generally solvent exposed and often involved in ion pairings, while most hydrophobic side chains were buried. The amino acid distribution within the HIP model is in good agreement with what is known from structural analysis of correctly folded proteins.

(3) Electrostatic Potential. Electrostatic potential calculations were carried out for the HIP model and the X-ray structure of the ATPase fragment of HSC70 (*37*). The DelPhi package (*38*), which solves the Poisson−Boltzmann equation by a finite difference method, was used for the calculation of the three-dimensional distribution of the electrostatic potential at physiological ionic strength and pH. The atomic coordinates were mapped into a three-dimensional grid with a resolution of about one grid point per angstrom. The grid was chosen to leave a 10 Å border between the protein and the grid edge. The dielectric constant was set to 4 for the protein interior and 80 for the surrounding solvent. Atomic radii definitions were taken from the DelPhi default param-

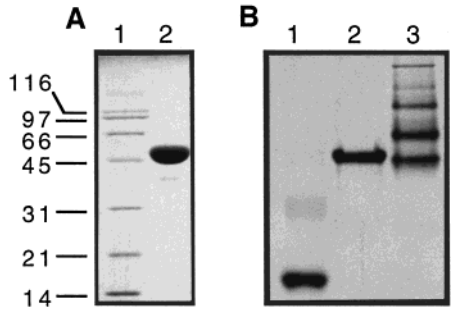

FIGURE 1: Analysis of the purified recombinant HIP by polyacrylamide gel electrophoresis (PAGE). (A) SDS−PAGE: lane 1, molecular mass markers (values in kilodaltons on the left); and lane 2, HIP (8 μg). (B) Native PAGE: lane 1, BSA (10 μg); lane 2, HIP (10 μg); and lane 3, HSC70 (30 μg).

eters (i.e., united atom scheme in which hydrogens are assigned a radius of 0.0 and the radii of carbon, nitrogen, and oxygen are slightly larger than normal to account for hydrogen atoms). A standard set of formal charges was assigned to the titratable residues (e.g., Arg + 1e, Lys + 1e, His + 0.5e, Asp − 1e, and Glu − 1e). Calculations with histidine residues considered neutral were also carried out, but as the electrostatic isosurfaces were similar to the ones obtained for His bearing a charge of 0.5e, we decided to select the latter computations. The N-terminal amino group and the C-terminal carboxy group were considered neutral. Similar calculations were performed with the X-ray structure of PP5 as a control. The solvent accessible surface was colored coded according to the electrostatic potential.

(4) Preliminary Docking. Interactive rigid-body docking was performed to generate possible HIP−HSC70 complexes. Overall shape and electrostatic complementarities were then considered to propose putative macromolecular complexes.

RESULTS

Purification and Chaperone Activity of HIP. HIP overproduced in *E. coli* has been purified to homogeneity and analyzed by polyacrylamide gel electrophoresis. Under denaturing conditions, the protein is 98% homogeneous, and although its molecular mass, calculated from its amino acid composition, is 43 545 Da, the protein behaves as a 51 000 Da species (Figure 1A) as reported previously (*16*). Under nondenaturing conditions, HIP appears to be a single species as compared to the multiple species observed for the polydisperse HSC70 (*27*) (Figure 1B).

HIP purified as described above is an active molecular chaperone, as it is able to inhibit the aggregation of unfolded rhodanese. As shown in Figure 2, unfolded rhodanese aggregates readily, as monitored by an increase in the level of light diffusion, when allowed to refold in refolding buffer. However, a significant inhibition of rhodanese aggregation occurs in the presence of an equimolar amount of HIP, and almost total inhibition is obtained at a 2/1 HIP/rhodanese molar ratio. This inhibition activity is specific to HIP since no significant effect is observed with BSA even at a BSA/rhodanese molar ratio of 20/1.

Conformational Properties of HIP. To obtain further information about the conformational parameters and molecular mass of HIP in solution, a combination of size-exclusion chromatography and sedimentation velocity analysis has been used. In size-exclusion chromatography, the

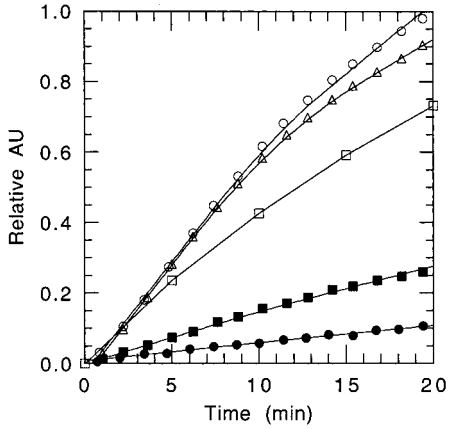

FIGURE 2: Effect of HIP on the aggregation of rhodanese. Rhodanese at a concentration of 50 μM was denatured and then allowed to refold in the presence or absence of HIP or BSA, as described in Experimental Procedures: rhodanese alone (○), 1/1 rhodanese/BSA (△), 1/20 rhodanese/BSA (□), 1/1 rhodanese/HIP (■), and 1/2 rhodanese/HIP (●). These values are based on the HIP monomer. Absorbance at 320 nm has been normalized to 1, based on the data of rhodanese alone (○) at 20 min (absorbance units).

protein elutes as a single sharp and symmetrical peak corresponding to a Stokes radius of 55 Å. This radius is too large for a globular monomer with a molecular mass of 43 500 Da, and corresponds in fact to a molecular mass of a globular protein of about 300 000 Da (Figure 3A).

Sedimentation velocity experiments confirmed the monodisperse nature of HIP as indicated by the presence of a single sharp boundary, whatever concentration was used. A g(s) representation (*28*), which shows the distribution of sedimenting species in a preparation and is very sensitive for detecting the presence of multiple species, gives a single sedimentation coefficient of about 2.8 S at the three concentrations that were used (Figure 3B). In fact, the HIP sedimentation coefficient decreases with concentration, as expected for a nonassociative, single particle, and an $s°$ of 2.83 S at 4 °C is obtained at infinite dilution (Figure 3B, inset). Correction of this value for temperature and solvent gives an $s°$ of 4.34 S at 20 °C, in water (Table 1). A similar $s°$ is obtained when the experiment is performed at 20 °C, indicating that HIP does not undergo a significant change in its shape or structure with increasing temperatures.

The use of the experimentally determined Stokes radius and sedimentation coefficient allows us to estimate the molecular mass to be about 101 000 Da, which is close to the molecular mass of a theoretical dimer (87 090 Da).

Quaternary Structure of HIP. To address more rigorously the quaternary structure of the protein, sedimentation equilibrium experiments were performed using three initial loading concentrations of HIP and three rotor speeds, resulting in nine data sets. Analysis of each data set separately for the determination of the weight-average molecular mass is reported in Figure 4. For the different rotor speeds, the weight-average molecular mass remains within a range of 81000−98000 Da over a large concentration range, indicating that the protein is essentially dimeric in solution. Fitting the nine data sets simultaneously using a single-ideal species model converges to a value of 88 284 Da (Figure 5 and Table 1), almost in exact agreement with the molecular mass for a theoretical dimer (87 090 Da).

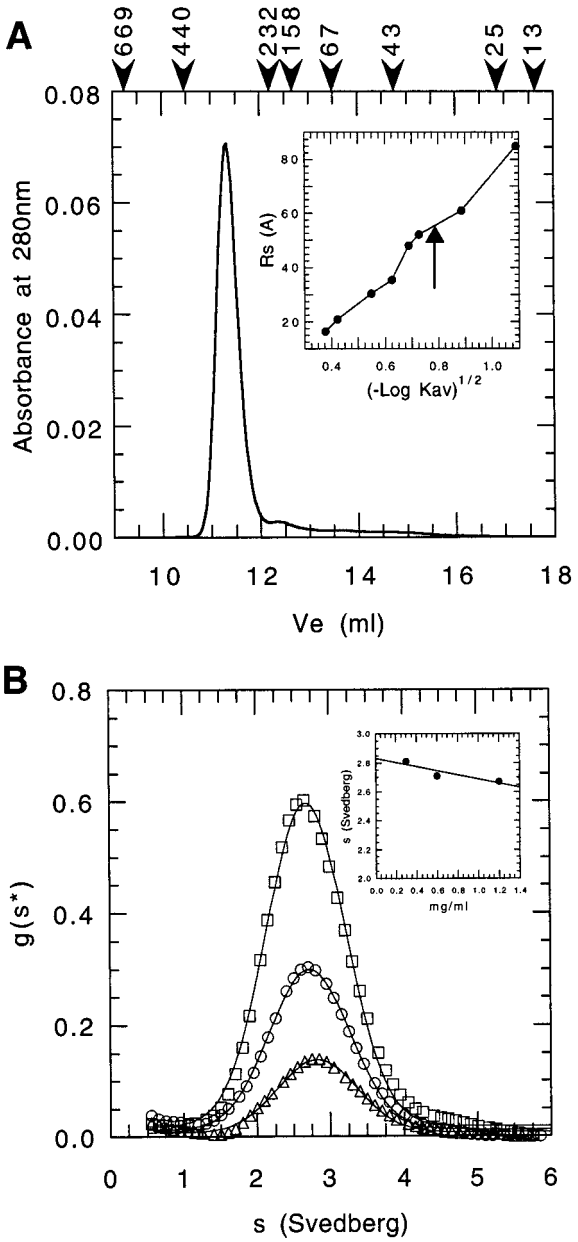

FIGURE 3: (A) Analysis of HIP by size-exclusion chromatography. One hundred microliters of protein at a concentration of 0.5 mg/mL was loaded on a Superdex 200 HR10/30 column and eluted as described in Experimental Procedures. In the inset, proteins with known molecular masses and Stokes radii were used for the calibration curve (●) representing the Stokes radius as a function of the distribution coefficient K_{av}. The arrow denotes to the distribution coefficient of HIP. (B) Analysis of HIP by sedimentation velocity. HIP at 0.3 (△), 0.6 (○), and 1.2 mg/mL (□) was sedimented, and the data were analyzed as described in Experimental Procedures. The curves of the fitted data according to Stafford (*23*) are represented by a solid line. The inset shows the variation of the sedimentation coefficient obtained at 4 °C as a function of HIP concentration. Comparable values of the sedimentation coefficient were obtained when the data were fitted directly to the Lamm equation according to Philo (*29*).

These data, combined with those from sedimentation velocity experiments, yield a frictional ratio f/f_0 of 1.6 for the HIP dimer (see Table 1), indicative of an important departure from spherical shape. The axial ratio a/b for the hydrodynamically equivalent prolate ellipsoid of revolution is calculated to be 11/1 for the anhydrous particle, and about 7.5/1 when a degree of hydration of 0.35 g of H_2O/g of protein is used.

Table 1: Hydrodynamic Parameters of HIP[a]

molecular mass (Da)	88 284 (87449−89123)
$s^\circ_{4,w}$ (S)	2.83 ± 0.1
$s^\circ_{20,w}$ (S)	4.34
f/f_0	1.6
a/b	7.5
R_s (Å)	55
$D_{20,w}$ (cm²/s)	3.83×10^{-7}

[a] The molecular mass is obtained by sedimentation equilibrium analysis, and numbers in parentheses represent the confidence interval given by the fitting procedure. The conformational parameters were calculated as described in Experimental Procedures, using the partial specific volume values determined from the amino acid composition. $s^\circ_{n,w}$ is the corrected sedimentation coefficient at a given temperature in water. f and f_o are the frictional coefficients. a/b is the axial ratio for the equivalent, hydrated, prolate ellipsoid of revolution. D is the corrected diffusion coefficient. R_s is the Stokes radius.

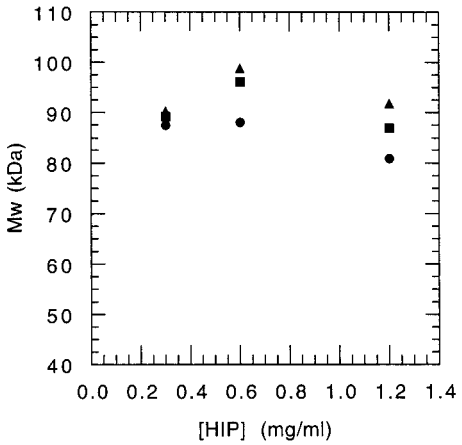

FIGURE 4: Variation of the weight-average molecular mass as a function of HIP concentration. HIP at various concentrations was centrifuged at 4 °C at 6000 (▲), 9000 (●), and 14 000 rpm (■) as described in Experimental Procedures. The weight-average molecular mass (MW) was obtained by fitting the data separately to a single-ideal species model.

Secondary Structure of HIP and Protein Modeling. Secondary structure prediction using several programs indicated that HIP is an almost all α-protein (Figure 6). These predictions are supported by the circular dichroism spectrum of the protein which shows a strong maximum at 190 nm and two strong minima at 208 and 222 nm, characteristic of α-helical structures (Figure 7). Analysis of the HIP circular dichroism data, by deconvolution of the spectrum as well as by direct comparison with myosin rod (100% of helices), indicates the presence of about 70% α-helical structure, 25% random coil, and 5% β-structure, in agreement with the prediction data. Moreover, the protein is predicted, using the "Coil" programs (*39*), to form coiled coils in the N-terminus and the region of residues 220−270 with high probability.

In an attempt to obtain information about the HIP three-dimensional structure, threading methods have been used to identify possible folds. This search identified the tetratricopeptide repeat (TPR) fold of protein phosphatase 5 (PP5) as the most likely fold for the TPR-containing region of HIP (residues 100−250). The Z-score for PP5, which ranked at the top of the fold library, was found to be 10.99, far above the confidence threshold Z-score for this method, which is 4.8 ± 1. As shown in Figure 6, the TPR-containing region

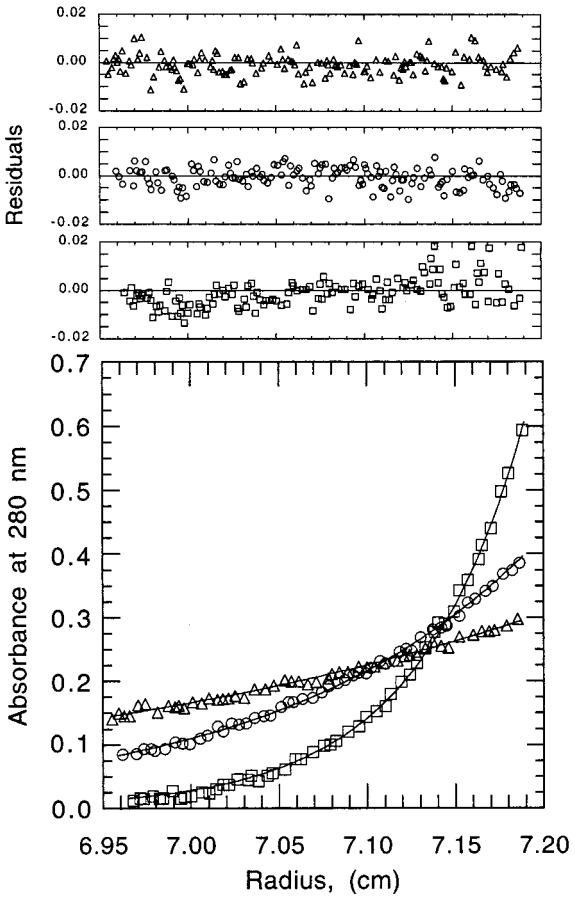

FIGURE 5: Analysis of HIP by equilibrium sedimentation analysis. Equilibrium sedimentation data obtained at 4 °C and 6000 (△), 9000 (○), and 14 000 rpm (□) using 0.3 (this figure), 0.6 (not shown), and 1.2 mg/mL (not shown) were fitted to a single-ideal species model as described in Experimental Procedures. The symbols represent the experimental data obtained at 0.3 mg/mL at the three rotor speeds, whereas the solid line is the result of the fit of each data set. The residuals representing the variation between the experimental data and those generated by the fit are shown.

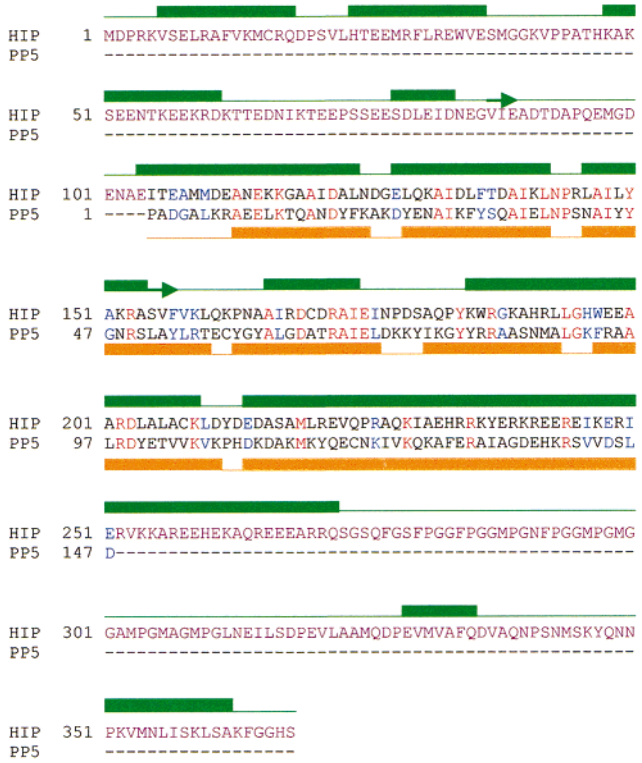

FIGURE 6: Secondary structure and amino acid sequence alignement of HIP and PP5. HIP and PP5 amino acid sequences were aligned on the NPS@ server of Pôle Bioinformatique Lyonnais (pbil.ibcp.fr). Identical residues are red, whereas conservative replacements are blue. The TPR region of HIP (residues 105−213) and that of PP5 (residues 20−127 of the authentic protein) are made by three pairs of α-helices, and are followed by a highly charged α-helix (residues 214−251 and 128−166 for HIP and PP5, respectively). The first residue of PP5 in the figure corresponds to residue 20 in the authentic protein. HIP secondary structure (green) was predicted using several programs found on the same server. PP5 secondary structure (orange) is that found in the three-dimensional structure (*35*). α-Helices are represented by rectangles, *β*-strands by arrows, and coils by lines.

of PP5 (residues 20−127) aligns very well on that of HIP (residues 105−213), and the helix that follows the TPR in PP5 (residues 128−166) is conserved in HIP (residues 214−251). Moreover, consensus TPR motif residues are conserved in both sequences. Thus, PP5 structure was used to build a model of the corresponding region in HIP. As shown in Figure 8A, the TPR region of HIP, made by six antiparallel helices, forms a groove that is flanked on the C-terminal side by a long α-helix. This α-helix, as well as the TPR region, has been reported previously to constitute the HSC70 binding domain (*16*, *17*). Therefore, electrostatic potential calculations for HIP and the ATPase domain of HSC70, followed by preliminary docking, were then carried out in an effort to identify potential interacting regions.

Interestingly, HIP exhibited a remarkable electrostatic surface, with an electropositive groove sandwiched between two protuberant electronegative regions, flanked by a long electropositive α-helix (Figure 8B, left). The electropositive groove contains residues K152, R153, K185, R187, K189, and R192. Beside lysine and arginine residues, the groove in HIP contains also a small cluster of hydrophobic and/or aromatic side chains that could be involved in protein−protein interactions. This small cluster involves I148, L193,

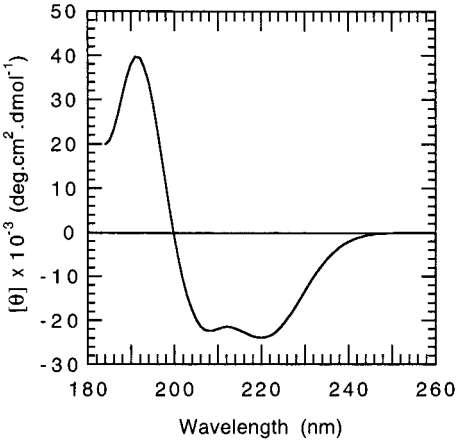

FIGURE 7: Analysis of secondary structure of HIP by circular dichroism. Molecular circular dichroism was measured using 4.6 *μ*M HIP as described in Experimental Procedures.

W186, L220, and M219. The electronegative regions flanking the groove contain residues D111, E112, E115, D122, and D126 on one side and a loop region centered on residues D211, D213, E214, and D215 on the other side.

The ATPase domain of HSC70, however, tends to be rather electropositive on one side of the nucleotide binding

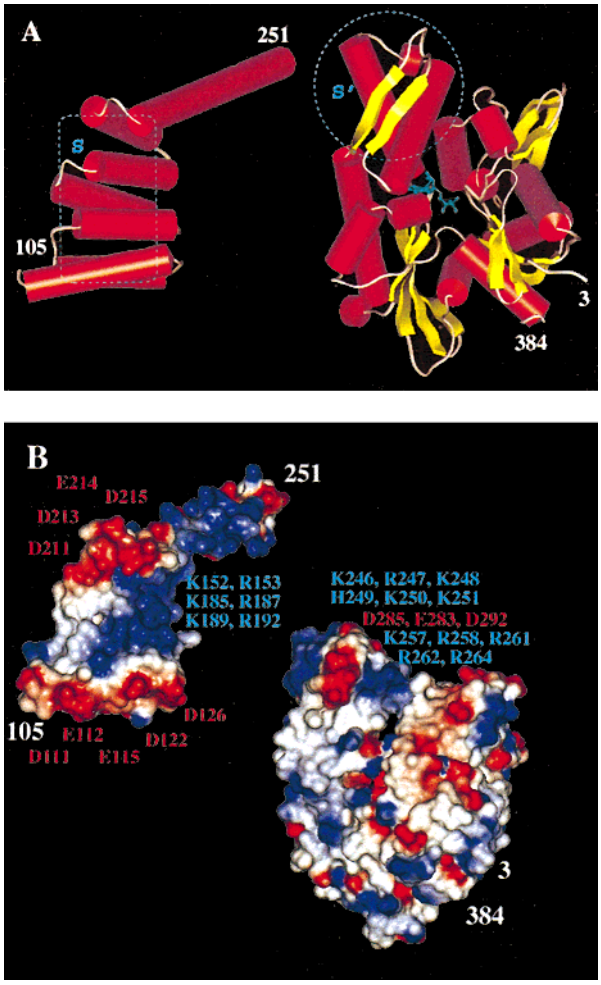

FIGURE 8: (A) Ribbon diagram for the TPR-containing region of HIP (left) and the ATPase fragment of HSC70 (right). Sites S and S′ suggested to form the binding sites are represented by a dashed line. The S site on HIP forms a groove, whereas the S′ site on HSC70-ATPase makes a protuberance. The nucleotide ADP, bound at the base of the cleft of the ATPase fragment of the HSC70, is shown in a ball-and-stick representation. (B) Molecular surface representation of the electrostatic potential of the HIP theoretical model (left) and the HSC70-ATPase X-ray structure (right). The orientation is similar to the one shown in panel A. The surfaces are color-coded according to electrostatic surface potential: red, -3 kcal mol^{-1} e^{-1}; white, 0 kcal mol^{-1} e^{-1}; and blue, 3 kcal mol^{-1} e^{-1}. The positions of charged side chains that may be involved in the HIP−HSC70 interaction are labeled for orientation.

cleft while more electronegative on the other side. Within the nucleotide binding region, the distribution of the electrostatic potential tends to be mosaic. Most importantly, a region located between residues 240−260 and 280−290 of HSC70 matches almost perfectly the region of HIP described above, not only in terms of shape but also with respect to electrostatic surface (Figure 8B, right). Docking this region to the TPR region of HIP reveals an interface area with favorable interactions. These regions may well constitute the binding sites on HIP and HSC70, and have been termed S and S′ accordingly (Figure 8A).

DISCUSSION

The results described above shed some light on the quaternary structure and gross conformation of HIP in solution, and give some information about the tertiary structure of the TPR region and about possible binding sites of HIP and HSC70.

Quaternary Structure. Although HIP has been described previously as a homo-oligomer, the oligomerization state of the protein remained unclear and tetrameric structures have been reported on the basis of size-exclusion chromatography (*14*, *40*). The protein behaves indeed as a single species corresponding to a globular protein with a Stokes radius of 55 Å and a molecular mass of about 200000−300000 Da on gel fitration (Figure 3A), which may be interpreted as a tetramer relative to the molecular mass calculated from the amino acid composition (43 545 Da). However, sedimentation velocity experiments indicate that this is not the case since HIP sediments as a single species at 4.34 S, which corresponds to a globular protein of about 60000−70000 Da rather than to a protein of 200 000 Da (Figure 3B).

These data correspond in fact to a smaller oligomeric structure having an unusual shape or hydration properties (see below), since a molecular mass of 101 000 Da could be calculated when the sedimentation coefficient and the Stokes radius are combined, suggesting that HIP is a dimer. In this respect, dimeric structures have previously been observed for HIP in cross-linking experiments (*16*). The dimeric nature of HIP is confirmed by sedimentation equilibrium, which allows the determination of molecular mass irrespective of shape. In this case, a value of 88 284 Da is obtained, in good agreement with the value of the molecular mass for a theoretical dimer (87 090 Da). Furthermore, whether at low concentrations, where it is reasonable to assume that the smallest stable species is present, or at high concentrations, the weight-average molecular mass never exceeded 98 000 Da, indicating that the protein is essentially dimeric in solution. The dimeric structure of HIP is consistent with the finding (*14*) that two HSC70 molecules are bound per HIP oligomer.

These conclusions are based on data obtained with a protein which differs from the authentic HIP by 18 residues (2270 Da), corresponding to the addition of a Myc epitope and a histidine tag at the C-terminal extremity (*14*). However, it is unlikely that the addition of such a tag may have affected the quaternary structure of the protein, since very comparable data (not shown) were obtained using an N-terminally tagged HIP, thus suggesting that the quaternary structure determined here is relevant of that of the authentic HIP.

Gross Conformation. The discrepancy observed between the molecular mass determined by size-exclusion chomatography and sedimentation velocity analysis (101 000 Da) and that by sedimentation equilibrium analysis (88 284 Da) suggests that HIP may be an asymmetric and/or an unusually hydrated particle. In fact, the frictional ratio f/f_0 of 1.6 calculated for the HIP dimer does suggest a departure from a spherical shape (see Table 1). However, since the frictional ratio depends on shape and hydration, the overall asymmetry of the molecule is better assessed by the axial ratio a/b for the hydrodynamically equivalent prolate ellipsoid of revolution. Using several plausible values of the degree of hydration ranging from 0.2 to 0.5 g of H_2O/g of protein, axial ratios of 8.6−6.4 were obtained (see also Table 1), thus confirming the asymmetric nature of the HIP dimer.

Although HIP appears to be essentially dimeric in solution, self-association at significantly high concentrations and/or intrinsic conformational heterogeneity may exist. This is indeed suggested by the presence of a small shoulder in the dc/dt data near an s of about 4−5 S at the highest HIP

concentration (Figure 3B) and the fact that excessively large values of *D* are obtained from the fitting procedure (not shown), even though the data fit well to a single species.

It has been reported previously that deletion of either the 14 (*16*) or the 38 (*17*) amino-terminal residues of HIP stabilizes a monomeric form that exhibits a normal molecular mass on gel filtration (*17*). If it is assumed that this mutant behaves as the entire 368-residue protein in terms of shape, it is reasonable to suggest that the HIP monomer is rather globular in shape, while the observed asymmetry is induced by dimerization of HIP, and is therefore a property of the dimer.

Tertiary Structure of the TPR Region of HIP. Although the TPR region of HIP and the highly charged segment following it (residues 100−270) have been involved in HSC70 binding (*16*, *17*), no structural information about interaction sites on both proteins has been reported. Since the crystallographic structure of PP5, a TPR-containing protein, is available, it was of interest to build the structure of the TPR region of HIP by comparative modeling. The subsequent determination of the electrostatic surface of the resulting model and that of the N-terminal domain of HSC70 would make it possible to define potential binding sites. The degree of sequence identity between the TPR region of HIP and that of PP5 is about 23%. However, secondary structure predictions, supported by circular dichroism data, indicated that these regions in HIP and PP5 are in fact very similar, in terms of secondary structure and consensus residues in the TPRs (see Figure 6). Furthermore, the fact that the amino acid distribution within the HIP final structural model was found to be in good agreement with that observed in correctly folded protein, and that no unusual structural features were noticed, supports the hypothesis that the TPRs of these two proteins are structurally very similar.

In the proposed three-dimensional model of the TPR of HIP, a well-defined shape and electrostatic surface are observed (Figure 8B, left). These features suggest that the electropositive groove forms a binding site because of its ability to attract a negatively charged region in another protein and to orient and fit in place the upcoming ligand with the help of the two prominent electronegative sides of the groove. To maintain strong protein−protein interactions, the floor of the groove is further lined with a few hydrophobic and/or aromatic residues, as often found within interaction site areas.

The solvent-exposed surface of HSC70, although essentially mosaic in terms of electrostatic potential, does exhibit a peculiar pattern around residues 240−260 and 280−290. A prominent electronegative region surrounded by two electropositive tracks makes what may be compared to a footprint of the TPR region of HIP. Thus, these two regions in HIP and HSC70 exhibit not only an overall shape complementarity but also an electrostatic complementarity. In fact, when the S region of HIP is docked onto the S′ region of HSC70, favorable interactions between charged residues of HIP and HSC70 are observed (see the Results and Figure 8). Most importantly, the proposed contact area between the two proteins, made essentially of salt links, is consistent with the observed sensitivity of the interaction between HIP and HSC70 to salt concentration (*16*), thus stressing the importance of electrostatic forces in HIP−HSC70 interactions. Moreover, the proposed binding site of HIP on HSC70, in the vicinity of the nucleotide binding cleft, is consistent with the effect of HIP on HSC70 nucleotide binding, namely, the stabilization of the ADP form. This region on HSC70 is almost the same as that which has been proposed to bind BAG-1, another cochaperone (*41*), and is in fact reminiscent of that of DnaK involved in binding GrpE (*42*), despite the structural differences between HIP, BAG-1, and GrpE. It is therefore tempting to speculate that residues 240−260 and 280−290 of HSP70 proteins may constitute a general and versatile binding site for cochaperones and other interacting proteins.

ACKNOWLEDGMENT

We are very grateful to Jorg Höhfeld and Ulrich Hartl for providing the plasmid expressing HIP used in this study and to Mohamed Rholam, Monique Monnot, and Serge Fermandjian for their help with the circular dichroism experiments and their interest in this study. We are also very grateful to Jean Lepault for the electronic microscopy and to Gérard Batelier for the analytical ultracentrifugation experiments.

REFERENCES

1. Hartl, F.-U. (1996) *Nature 381*, 571−579.
2. Schatz, G., and Dobberstein, B. (1996) *Science 271*, 1519−1526.
3. Bukau, B., and Horwich, A. L. (1998) *Cell 92*, 351−366.
4. Bohen, S. P., Kralli, A., and Yamamoto, K. R. (1995) *Science 268*, 1303−1304.
5. Orsini, G., and Goldberg, M. E. (1978) *J. Biol. Chem. 253*, 3453−3458.
6. Zettlmeissi, G., Rudolph, R., and Jaenicke, R. (1979) *Biochemistry 18*, 5567−5571.
7. Kiefhaber, T., Rudolph, R., Kohler, H. H., and Buchner, J. (1991) *Bio/Technology 9*, 825−829.
8. Randall, L. L., and Hardy, J. S. (1995) *Trends Biochem. Sci. 20*, 65−69.
9. Palleros, D. R., Reid, K. L., Shi, L., Welch, W. J., and Fink, A. L. (1993) *Nature 365*, 664−666.
10. Greene, L. E., Zinner, R., Naficy, S., and Eisenberg, E. (1995) *J. Biol. Chem. 270*, 2967−2973.
11. McCarthy, J. S., Buchberger, A., Reinstein, J., and Bukau, B. (1995) *J. Mol. Biol. 249*, 126−137.
12. Cyr, D. M., Langer, T., and Douglas, M. G. (1994) *Trends Biochem. Sci. 19*, 176−181.
13. Stuart, R. A., Cyr, D. M., Craig, E. A., and Neupert, W. (1994) *Trends Biochem. Sci. 20*, 87−92.
14. Höhfeld, J., Minami, Y., and Hartl, F. U. (1995) *Cell 83*, 589−598.
15. Prapapanich, V., Chen, S., Nair, S. C., Rimerman, R. A., and Smith, D. F. (1996) *Mol. Endocrinol. 10*, 420−431.
16. Prapapanich, V., Chen, S., Toran, E. J., Rimerman, R. A., and Smith, D. F. (1996) *Mol. Cell. Biol. 16*, 6200−6207.
17. Irmer, H., and Hohfeld, J. (1997) *J. Biol. Chem. 272*, 2230−2235.
18. Ziegelhoffer, T., Johnson, J. L., and Craig, E. A. (1996) *Curr. Biol. 6*, 272−275.
19. Frydman, J., and Hohfeld, J. (1997) *Trends Biochem. Sci. 22*, 87−92.
20. Hohfeld, J., and Jentsch, S. (1997) *EMBO J. 16*, 6209−6216.
21. Gross, M., and Hessefort, S. (1996) *J. Biol. Chem. 271*, 16833−16841.
22. Laemmli, U. K. (1970) *Nature 227*, 680−685.
23. Kim, D., Lee, Y. J., and Corry, P. M. (1992) *J. Cell. Physiol. 153*, 353−361.
24. Siegel, L. M., and Monty, K. J. (1966) *Biochim. Biophys. Acta 112*, 346−362.

25. Le Maire, M., Rivas, E., and Moller, J. V. (1980) *Anal. Biochem. 106*, 12−21.
26. Zhong, L., and Johnson, W. C. (1992*) Proc. Natl. Acad. Sci. U.S.A. 89*, 4462−4465.
27. Benaroudj, N., Batelier, G., Triniolles, F., and Ladjimi, M. M. (1995) *Biochemistry 34*, 15282−15290.
28. Stafford, W. F. (1994) *Modern analytical ultracentrifugation: acquisition and interpretation of data for biological and synthetic polymer systems*, pp 119−137, Birkhäuser, Boston.
29. Philo, J. S. (1994) *Modern analytical ultracentrifugation: acquisition and interpretation of data for biological and synthetic polymer systems*, pp 156−170, Birkhäuser, Boston.
30. Laue, T. M., Shah, B. D., Ridgeway, T. M., and Pelletier, S. L. (1992) in *Analytical Ultracentrifugation in Biochemistry and Polymer Science* (Harding, S. E., Rowe, A. J., and Horton, J. C., Eds.) pp 90−125, The Royal Society of Chemistry, Cambridge, U.K.
31. Kuntz, I. D. (1971) *J. Am. Chem. Soc. 93*, 514−516.
32. Lin, T.-H., Quinn, T., Walsh, M., Grandgenett, D., and Lee, J. C. (1991) *J. Biol. Chem. 266*, 1635−1640.
33. McRorie, D. K., and Voelker, P. J. (1993) *Self-associating systems in the analytical ultracentrifuge*, Beckman Instruments Inc.
34. Fischer, D., and Eisenberg, D. (1996) *Protein Sci. 5*, 947−955.
35. Das, A. K., Cohen, P. T. W., and Barford, D. (1998) *EMBO J. 17*, 1192−1199.
36. Ponder, J. W., and Richard, F. M. (1987) *J. Mol. Biol. 193*, 775−785.
37. Flaherty, K. M., De-Luca-Flaherty, C., and McKay, D. B. (1990) *Nature 346*, 623−628.
38. Sharp, K., and Honig, B. (1990) *Annu. Rev. Biophys. Biochem. 19*, 301.
39. Lupas, A., Van Dyke, M., and Stock, J. (1991) *Science 252*, 1162−1164.
40. Bruce, B. D., and Churchich, J. (1997) *Eur. J. Biochem. 245*, 738−744.
41. Stuart, J. K., Myszka, D. G., Joss, L., Mitchell, R. S., McDonald, S. M., Xie, Z., Takayama, S., Reed, J. C., and Ely, K. R. (1998) *J. Biol. Chem. 273*, 22506−22514.
42. Harrison, C. J., Hayer-Hartl, M., Di Liberto, M., Hartl, F.-U., and Kuriyan, J. (1997) *Science 276*, 431−435.

BI9917535